An Embedded System for Quasi Real-time Lighting Computation based on Sky Monitoring

Yujie Wu[1], Jérôme Henri Kämpf[2], Jean-Louis Scartezzini[1]

[1]Solar Energy and Building Physics Laboratory (LESO-PB),
École polytechnique fédérale de Lausanne (EPFL), CH-1015, Lausanne, Switzerland
[2]Haute école d'ingénierie et d'architecture Fribourg (HEIA-FR), CH-1705, Fribourg, Switzerland

Abstract

Lighting simulation plays a significant role in the architectural design and evaluation of performance parameters of buildings. The general method of assuming a virtual sky in lighting simulation may lead to mismatch with the real situation, which conventionally ignores or approximates the complexity of the real sky and surrounding landscape in luminance distribution. In this paper, we propose a compact embedded system for on-board quasi real-time lighting computation based on sky monitoring and luminance mapping.

The embedded system comprises a microprocessor and a calibrated low-cost image sensor with a wide-angle lens. The luminance detection range of the device, by employing the high dynamic range (HDR) technique, is able to cover 7 orders of magnitude in luminance monitoring including that of the sun, sky and ambient objects during daytime. The monitored luminance can be mapped to 1.23 million sky patches, achieving high resolution of the sky and ground dome. Taking the outdoor luminance map as input, the microprocessor conducts the on-board lighting computation by RADIANCE program based on ray-tracing algorithms. This integrated embedded system is demonstrated to accomplish an intra-scene lighting computation in a quasi real-time manner based on the monitored sky and ambience.

Keywords: Real-time, Sky monitoring, Luminance mapping, FPGA, Embedded System

Introduction

In Switzerland, 12% of the electrical energy is consumed by artificial lighting every year (SFO (2013)). Maximizing the use of daylight has become a trend in the architectural design to mitigate the need for artificial lighting which, at the same time, will potentially improve occupants' visual comfort and non-visual health (Ochoa et al. (2012)). The proliferation of lighting simulation is playing a significant role in design, performance analysis and engineering aspects of architecture. Nonetheless, majority of the daylight simulation was based on unelaborated assumptions of the sky, weather or environmental conditions instead of field measurement (Ochoa et al. (2012)), which can contribute to noticeable bias in the following ways. Firstly, the coarse assumptions of a CIE sky model with a smooth luminance distribution would contribute to a substantial discrepancy from the real sky, ignoring the mutable patterns of clouds and Rayleigh scattering effect of the sky (Wittkopf and Soon (2007)). Secondly, although the maximum solar luminance is predictable (1.6×10^9 cd/m^2), the atmosphere condition is variable: mist, haze or smog can attenuate the luminance of the sun and sky substantially (Ferraro et al. (2011)). In addition, as the position of the sun approaches close to the horizon, the increased transversal distance of solar light through the atmosphere is another factor impairing its intensity reaching the ground. Although the Perez All-weather model (Perez et al. (1993)) is able to predict a sky based on inputs from measurement of direct normal and diffuse horizontal illuminance, it is still insufficient to model the real complexity of a sky by sampling two inputs and interpolation. Studies show noticeable inaccuracy especially in vertical illuminance evaluation (Mardaljevic (1999)). Last but not least, oversimplification on the ambience of a scene model frequently fails to evaluate glare sources from the real surrounding landscape, for instance, from light pollution - veiling reflection of direct solar rays on a glazing wall of a neighbouring building or on a windscreen of a static vehicle (Su et al. (2013)). The above mentioned simplification of scene modelling can be potentially improved by the real-site monitoring with substantial augmentation of the number of inputs (high sampling rate of the sky and ambience). Nonetheless, the real-site monitoring is limited to the dynamic range of a device to cover both the sky and ambient objects at the same time, as the difference between the luminance of the sun (about 1.6×10^9 cd/m^2) and that of objects in shadow ($10 - 100$ cd/m^2) is tremendous. Apart from this, the resolution of the sky patches and the time consumption for bulky computation on an embedded platform are among the many factors challenging the real-site lighting simulation.

With the technological development and popu-

larity of vision sensors, the high dynamic range (HDR) imaging technique has started to be applied in photography and computer vision and, in the recent years, has been elucidated to be viable as an apparatus for photometric measurement. Stumpfel et al. (2004) employed a high-end digital single-lens reflex (DSLR, Canon-1Ds) camera coupled with a wide-angle lens (180°) and a laptop to capture images of the sky. In this scheme, although 7 frames synthesized a HDR image covering 4 million times (132 dB) of light intensity for the sun and the sky during daytime, the dynamic range was still not wide enough to capture relatively dim environmental objects. And as the work focused on photo-realistic rendering, it did not address photometric physical quantities such as illuminance and luminance. Wüller and Gabele (2007) proposed another way of using a DSLR camera to measure photometric quantity as a luminance meter. By converting the RGB gray-scale value to the XYZ color space by a linear mapping matrix, the system was able to output luminance value. In spite of the consideration of ISO setting and vignette, neglecting mismatch between the real RGB spectral response of the image sensor and the standard RGB color matching function, the system had noticeable error when measuring colored objects. In addition, each alternation of the aperture of a DSLR lens led to a change in vignette, adding on further complexity to calculation and calibration process. Borisuit et al. (2012) employed a high dynamic range camera as a tool for intra-scene luminance mapping. The dynamic range of the image sensor reaches 132 dB and three pieces of glass filter were used to correct the spectral response of the black and white image sensor. However, a single frame of 132 dB dynamic range could hardly cover the wide luminance range requirement in outdoor applications ($>$ 150 dB) for monitoring the sun and ambient objects at the same time. And HDR image sensors, in general, sacrifice the resolution for large pixel size on the silicon wafer and their cost is relatively high under the contemporary technology of fabrication.

In this paper, we try to employ a field-programmable gate array (FPGA) chip to control a low-cost image sensor to build up a compact embedded-system that is highly integrated with quasi real-time lighting simulation and measurement of the luminance of the sun, sky and ambient objects, covering a broad dynamic range. In this way, the input to the lighting computation is based on the measurement of luminance distribution instead of interpolation or assumption of a simple sky. At the same time, its capability of on-board quasi real-time lighting simulation of a scene can be further extended and potentially applied in photo-realistic rendering, evaluation of lighting performance parameter and building automation.

Anatomy of the system

From the hardware perspective, an image sensor, a fish-eye lens, a microprocessor (FPGA) and 1 Gigabyte memory comprise the device, establishing a highly integrated embedded-system independent of any external computation platform.

Imaging system

A low-cost digital image sensor was employed as a major detector in this platform. The 1/2.5 inch complementary metal oxide semiconductor (CMOS) image sensor is featured with 5 million pixels (2592×1944), 38.1 dB signal to noise ratio (SNR) and 12-bits analog to digital converter (ADC). The sensor is a low power consuming device with maximum power at 381 mW. A wide operating temperature from -30 °C to 70 °C allows it to work in majority of geographical locations and seasons on the Earth.

The image sensor is coupled with a wide-angle lens of focal length at 2.5 mm, ensuring that the field of view (FOV) of the imaging system covers major area of the sky dome and surrounding landscape. The reason we did not employ wider angle lens lies in the consideration of keeping the distortion at tolerable scale, as extreme wide-angle lens tends to suffer from apparent radical and tangential distortions, which aggravates complexity in post-calibration. For this device, the imaging system spans a view angle of $129.8° \times 96.8°$ in horizontal and vertical directions respectively and the maximum is 162.5° in the diagonal direction. In addition, a short-pass filter and a long-pass filter were placed between the lens and the image sensor to correct its spectral response according to CIE photopic luminosity function $V(\lambda)$ making the image sensor to be photometrically correct (f1' error 19.3%). The vignette and geometric distortions of the fish-eye lens were also measured and calibrated to ensure the mapping accuracy (Wüller and Gabele (2007)).

Considering the extreme intensity of the solar rays, an opaque shield was positioned in front of the lens to protect the image sensor and, at the same time, it is controlled by a stepper motor to automatically open the shield at the moment of image capturing and synchronously close when it finishes. The maximum open time is 0.55 seconds securing that the image sensor will not be overheated during this short period by the intensive direct-solar rays, mitigating the risk of irreversible physical damage to pixels.

Processor

The microprocessor (FPGA) and 1 Gigabyte external memory constitute the hub for logic control and

computation. As an embedded system, its power dissipation, compactness and computing power are among the major concerns. Due to its highly customizable feature as an economical solution in non-recurring engineering (Simpson (2010)), we adopted a single FPGA-SoC (system on chip) microprocessor to accomplish tasks including precise control of sensors and actuators, synthesis in HDR imaging, luminance mapping and on-board lighting computation. The FPGA chip (Altera Cyclone V) integrates two major parts on a single silicon die: the FPGA fabric part and hard core processor (HPS) part. The FPGA fabric part is a massive area of programmable gate arrays (85K logic cells) preferable in parallel computing and control of sensors. In this paper, we limited the FPGA fabric to the control of image sensor and stepper motor for occluding lens from the sky or the sun and will put the optimization in parallel computation into the future work. The HPS part is mainly composed of an ARM Cortex-A9 dual core processor working at 925 MHz together with communication bridges with the FPGA fabric. In this paper, it is designed to be in charge of relatively high level algorithms including the synthesis in HDR imaging, luminance mapping of the scene and lighting simulation. The configuration of the modules implemented in the FPGA and associated peripheral components are illustrated in Figure 1.

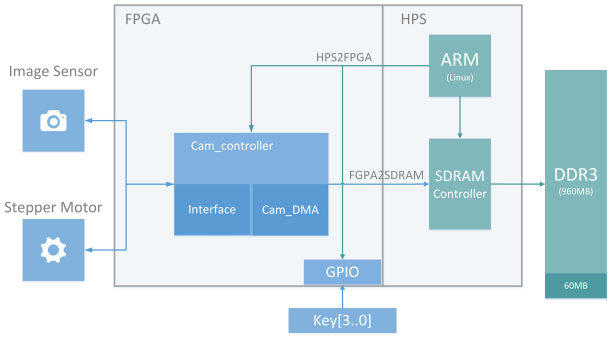

Figure 1: Modules configured in an FPGA chip

The FPGA fabric feeds the image sensor with a high frequency clock operating at 96 MHz to drive the sequential output of pixels. Together with multiple internal counters, the processor is able to control the exposure time of the image sensor ranging from microseconds upto minutes. Based on the consideration of capturing images of rapid moving clouds, the maximum exposure time was limited to 500 ms to avoid blurring.

Although the 12-bits ADC of the image sensor outputs 1-4096 levels of discrete gray-scale value, we filter out values outside the linear region of pixels and keep only 40-3100 to be the valid range, at the same time, excluding dark current noise and reset noise of the sensor. In this way, the brightest pixel receives > 64 times more photons than that of the dimmest pixel on the same frame. When 5 consecutive frames are taken with effective exposure time ranging from 1 μs upto 500 ms, the synthesized luminance spans 7 orders of magnitude (about 3.1×10^7, 150 dB), which would be sufficient to cover the range of luminance of the direct solar radiation (10^9 cd/m^2) and that of environmental objects (≥ 100 cd/m^2) in daytime.

Testing method

In order to assess its accuracy, we tested the device to measure the luminance at the exit port of an integration sphere and compare the value with the measurement of a class B luminance meter as a reference (f1' error 8%). The reason for employing an integration sphere is due to the mismatch between the FOV of a luminance meter and that of a single pixel on image sensor. The FOV of the luminance meter (Minolta LS-110) is about 0.33° while the equivalent resolution of a single pixel is 0.041° (subtends 5.24×10^{-7} sr in solid angle), of which the difference is considerable. And this also explains the image sensor possesses supreme resolution in detecting glare sources especially in small size for occupants, compared with a luminance meter. Therefore, an integration sphere was used to diffuse the beam of a light source homogeneously after multiple times of reflection (approximated as Lambertian reflection) and its directional luminance is thus assumed constant (within a limited region). In this way, despite of the gap between the resolution of the two devices, the target luminance is essentially identical due to the homogeneous nature of the integration sphere.

The set up of the experiment is presented in Figure 2. The luminance meter was placed on the left side next to the device under test, which were both aligned to target at the adjacent regions in the integration sphere. On the right side, it was an arc light source (Xenon, 1000 W) together with a power regulator, shedding an intensive light beam into the sphere. Additionally, the set-up was placed in an enclosed dark chamber, excluding parasitic light.

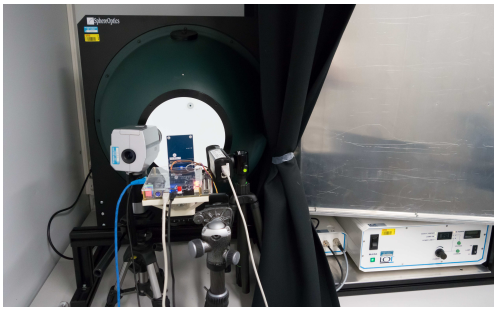

Figure 2: Experimental set-up

The power and aperture of the light source were adjusted to tune the luminance at the exit port of the integration sphere ranging from 15 to 350 cd/m^2. And 102 data points were collected for comparison with the reading from the reference luminance meter. For each point, 5 measurements were repeated to average out the temporal noise at time interval of 20 ms and 9 pixels were taken into calculation to reduce the spatial noise. Figure 3 shows the relative error of the device over the reference measurement of the luminance meter, where majority of the monitored luminance value concentrate within regions of $\pm 2\%$ error. Due to the linearity between the exposure time and luminance (number of photons), the error is applicable to other exposure times for gray-scale values in the linear range.

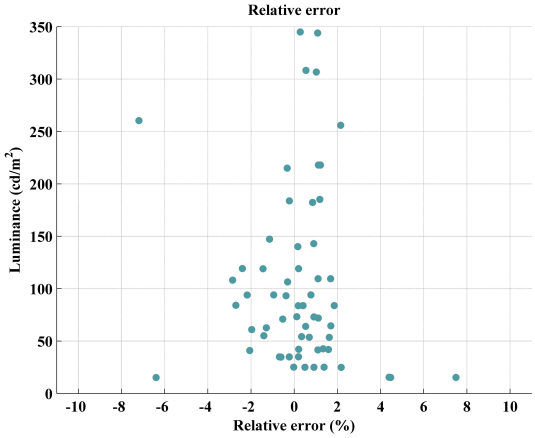

Figure 3: Relative error of measured luminance

Luminance mapping and lighting simulation

Merging every 4 pixels of RGB channels as a group, the device is able to output 1.23 million cells of luminance value and each cell corresponds to an unique directional angle of an incident ray. Therefore, we can map the luminance values from the image plane to 1.23 million patches of the sky or ground dome. As the focal length of the lens is infinitesimal compared with the distance between the device and environmental objects, such as neighbouring buildings, gardens and static vehicles, we approximate both ambient objects and the sky to be at infinite distance from the lens and virtually immerse the environmental objects into the infinite sky and ground dome, regarding them, including clouds and the sun, to be one integrated entity in mapping.

The microprocessor is able to accomplish the control of HDR imaging and luminance mapping within 1.3 seconds. The mapped luminance of the sky and objects is stored in a .cal file as input to the RADIANCE in lighting simulation. For the lighting computation of a room with unilateral façades, one half of the sky hemisphere, that the window is facing towards, induces as the source of lighting, together with one half of the ground hemisphere with ambient objects. In the light of this, one hemisphere of the sky and ground dome, in sum, faced by the façade of the room is sufficient for luminance monitoring and lighting simulation for a scene with unilateral façades. Therefore, the device can be positioned in front of the window glazing to perform the monitoring and lighting computation, ensuring the axis of lens aligned in the same direction as that the window glazing is facing towards.

We employed the RADIANCE program to compute the lighting in an office room, based on back-ward ray tracing algorithm. A scene of an office was created and then the microprocessor synthesises the monitored luminance of the sky and ground half-hemisphere together with the scene of the office room into an octree file, which is taken as an input for lighting computation. Afterwards, the rtrace and rpict, sub-programs of RADIANCE, operate on the HPS part of the FPGA chip to generate the rendering and calculate the luminance and illuminance distribution inside the room.

Figure 4 presents the rendering of a reference office on a sunny day, with monitored luminance of the sky, the sun and ambient objects as input. The contour of the surrounding buildings and trees exhibits clearly on the rendered image from a view point inside the room facing towards outside, due to high resolution mapping. As only photometric quantity get involved, the color of light source is ignored and thus the sky and surrounding landscape appear gray. For tracing 1.41×10^6 rays, it takes 79.2 seconds to accomplish the rendering on the HPS part of the processor with 1.23 million mapped sky or ground patches as input.

Figure 4: Rendering of a reference office room

The number of mapped patches influences the computation time for rendering remarkably. If employing 145 Tregenza sky patches, the rendering time reduces to 1/3 (20-30 s). On the other hand, the calculation of horizontal illuminance distribution consumes relatively less, 10 s for direct calculation of 400 virtual illuminance sensors. Moreover, increasing the number of tracing rays would eliminate the splotchy pattern on the wall and generate clear shadows as Figure 5 b), but it would also contribute to increment of computation period accordingly. For comparison, the rendering of the same scene by employing Perez sky model was presented in Figure 5 a), of which the direct normal and diffuse horizontal irradiance were measured on the roof of the laboratory at the same time as Figure 5 b). Apart from the surrounding landscape view at the glazing, there are differences in the figures about the shadow of the sun on the table, as the sun was occluded by thin clouds at that time.

Figure 5: Rendering by a) Perez model b) Embedded device

Conclusion

The paper proposed an embedded system (Patent pending) integrating quasi real-time sky monitoring and lighting computation based on a microprocessor and a low-cost image sensor. With HDR imaging technique, the device is able to monitor luminance covering 7 orders of magnitude (150 dB). The monitored luminance of the sky and ambient landscape can be mapped up to 1.23 million patches, achieving high resolution of the sky and ground for ultra-small glare source detection. Additionally, as the device monitors, in relative position, the sky and ground dome that a façade is facing to, establishing relative coordinates, it is unnecessary for a pre-knowledge of the orientation, geographical position, or weather condition for a unilateral-façade room for lighting computation. The rendering on the HPS part of the device takes 79.2 s for maximum resolution of sky patches and tracing 1.4 million rays, while illuminance distribution consumes 10 s for 400 points of virtual sensors. If certain application imposes requirement on computation time, the 5-phase method can be alternatively employed to boost computation speed of vertical or horizontal illuminance by using pre-computed matrices (Bourgeois et al. (2008)).

With its field measurement (real-site) and high-resolution luminance mapping of the sky and ground dome including surrounding landscape, the device may shows its merits in applications of photo-realistic rendering and evaluation of intra-scene lighting performance on illuminance level, uniformity of luminance distribution and glare assessment. The device may also be potentially applied in building automation due to its compactness, short time response and integration of luminance measurement together with lighting simulation as an embedded system. As the FPGA fabric part of the processor provides massive logic gate arrays for parallel computing, we will work on the optimization of computing logic of FPGA to boost the calculation speed in our future work. In addition, it would be interesting to compare the error between the computed illuminance distribution from this device and measured value by a reference illuminance meter (field verification) in a real office module.

Acknowledgements

The authors would like to thank the Commission for Technology and Innovation of Switzerland for funding Swiss Competence Center for Energy Research (SCCER), Future Energy Efficiency Buildings and District (FEEB&D).

References

Borisuit, A., M. Münch, L. Deschamps, J. Kämpf, and J.-L. Scartezzini (2012). A new device for dynamic luminance mapping and glare risk assessment in buildings. Volume 8485, pp. 84850M–84850M–9.

Bourgeois, D., C. F. Reinhart, and G. Ward (2008). Standard daylight coefficient model for dynamic daylighting simulations. *Building Research & Information 36*(1), 68–82.

Ferraro, V., M. Mele, and V. Marinelli (2011). Sky luminance measurements and comparisons with calculation models. *Journal of Atmospheric and Solar-Terrestrial Physics 73*(13), 1780 – 1789.

Mardaljevic, J. (1999, Dec). *Daylight Simulation:Validation, Sky Models and Daylight Coefficients*. Ph. D. thesis, Montfort University Leicester.

Ochoa, C. E., M. B. Aries, and J. L. Hensen (2012). State of the art in lighting simulation for building science: a literature review. *Journal of Building Performance Simulation 5*(4), 209–233.

Ochoa, C. E., M. B. Aries, E. J. van Loenen, and J. L. Hensen (2012). Considerations on design optimization criteria for windows providing low energy

consumption and high visual comfort. *Applied Energy 95*, 238 – 245.

Perez, R., R. Seals, and J. Michalsky (1993). Allweather model for sky luminance distributionpreliminary configuration and validation. *Solar Energy 50*(3), 235 – 245.

SFO (2013). Analyse des schweizerischen energieverbrauchs 2000-2012 nach verwendungszwecken. Technical report, Swiss Federal Office of Energy.

Simpson, P. (2010). *FPGA Design - Best Practices for Team-based Design*. Springer New York.

Stumpfel, J., C. Tchou, A. Jones, T. Hawkins, A. Wenger, and P. Debevec (2004). Direct hdr capture of the sun and sky. In *Proceedings of the 3rd International Conference on Computer Graphics, Virtual Reality, Visualisation and Interaction in Africa*, AFRIGRAPH '04, New York, NY, USA, pp. 145–149. ACM.

Su, X. M., M. Y. Zhang, and Z. G. Hao (2013, 12). China's streets lighting environment impact factors analysis. In *Sustainable Development and Environment II*, Volume 409 of *Applied Mechanics and Materials*, pp. 1036–1039. Trans Tech Publications.

Wittkopf, S. K. and L. K. Soon (2007). Analysing sky luminance scans and predicting frequent sky patterns in singapore. *Lighting Research and Technology 39*(1), 31–51.

Wüller, D. and H. Gabele (2007). The usage of digital cameras as luminance meters. *Proc. SPIE 6502*, 65020U–65020U–11.